The Effect of Microstructural Banding on Failure Initiation of HY-100 Steel

D. CHAE, D.A. KOSS, A.L. WILSON, and P.R. HOWELL

Microstructural banding of a hot-rolled HY-100 steel plate was accentuated by cooling slowly from the austenite region, which resulted in alternating layers of soft, equiaxed ferrite, and hard "granular ferrite." The segregation of substitutional alloying elements such as Ni and Cr was identified as the main cause for the microstructural banding. Such banding induces anisotropic flow behavior at large strains, with deformation constrained by "pancake-shaped" bands of the hard granular ferrite. Tensile tests of circumferentially notched HY-100 specimens were performed in order to explore the stress dependence of failure in the slow-cooled as well as the quenched and tempered conditions. The failure behavior of the slow-cooled, microstructurally banded material exhibited a pronounced susceptibility to a void-sheet mode of failure. However, the absence of carbides within the equiaxed ferrite delays void coalescence and material failure to higher strains than in a quenched and tempered microstructure, despite the increased susceptibility to shear localization.

I. INTRODUCTION

MICROSTRUCTURAL banding of hot-rolled, low-alloy steels is a common occurrence and is associated with the chemical banding of substitutional alloying elements.[1–5] The phenomenon can be understood in terms of the decomposition modes of the chemically inhomogeneous austenite under certain combinations of grain size and cooling rate.[4,5] For example, when these steels are slowly cooled from the austenite region, proeutectoid ferrite first forms within those regions, where the content of austenite-stabilizing elements is relatively small. The subsequent growth of proeutectoid ferrite creates essentially carbide-free regions within the microstructure. Finally, pearlite forms in the region of high solute (austenite stabilizer) content, thus creating a banded microstructure consisting of pearlite and ferrite bands.

The HY-100 steel may be characterized as a hardenable steel which depends on Ni, Cr, Mn, and Mo contents for hardenability. Considering that the chemical banding gives rise to the microstructural banding, and given the relatively high content of the substitutional alloying elements, HY-100 is expected to show a high susceptibility to microstructural banding. Microstructural banding has not been previously studied in HY-100 steel. Furthermore, while the phase transformations associated with microstructural banding have been studied in some detail in low-alloy steels, the few reports of the mechanical properties of microstructurally banded steels[6,7] are limited to the effects on tensile ductility and impact resistance.[6] None of the previous research has addressed the issue of the effect of microstructural banding on the micromechanism of failure at a high-stress triaxiality.

The tensile-failure behavior of a quenched and tempered HY-100 steel plate has recently been examined as a function of the stress state.[8,9,10] The results of these studies show that, for loading parallel to the long transverse direction of the plate, failure at high-stress triaxialities occurs as a result of localized shear deformation, as voids link due to a void-sheeting mechanism.[8,9,10] Such failure has been shown to depend on the presence of elongated MnS inclusions, which are oriented normal to the tensile axis and which nucleate large, elongated, cylindrically shaped voids. Material separation subsequently occurs as shear localization develops between the elongated, primary voids, resulting in the formation of carbide-nucleated secondary voids. In such a failure process, the carbides serve as secondary void sites but are active in initiating voids only after large local strains are induced, due to deformation localization in the ligament between the primary voids. Therefore, void-sheet failure may be delayed, but not avoided, if the nucleation of voids at carbides is suppressed. An extreme method for suppressing the void initiation at carbides is to produce carbide-free ligaments between the elongated MnS inclusions. For this purpose, we have used a slow-cool heat treatment to induce a banded microstructure containing bands of essentially carbide-free ferrite within the HY-100 steel.

The present study examines the effect of microstructural banding on the failure initiation of HY-100 steel. We focus on the formation of a banded microstructure and how such a microstructure affects failure of HY-100 steel at a high-stress triaxiality, such as in a notched or cracked plate. Previous research has suggested that, in the quenched and tempered condition, the failure of HY-100 can be limited by the intervention of a void-sheet mode of void linking, as opposed to one in which equiaxed voids grow in a more-or-less stable manner to coalescence. In the present study, we introduce a banded microstructure, consisting of alternating bands of soft, equiaxed ferrite and hard, granular ferrite, obtained by slow cooling (furnace cooling) of the as-received HY-100 plate. We also present results that indicate a strain-induced "anisotropic" flow behavior of the microstructurally banded material and contrast the failure strains over a range of stress triaxialities to those from an "unbanded" quenched and tempered HY-100 steel.

D. CHAE and A.L. WILSON, Graduate Research Assistants, and D.A. KOSS and P.R. HOWELL, Professors, are with the Department of Materials Science and Engineering, The Pennsylvania State University, University Park, PA 16802.

Manuscript submitted August 4, 1999.

Table I. Chemical Compositions of the HY-100 Steel Plate

Wt Pct	C	Mn	P	S	Si	Ni	Cr	Mo	Cu
HY-100	0.16	0.26	0.008	0.009	0.22	2.62	1.32	0.25	0.14

II. EXPERIMENTAL PROCEDURE

The material used in this study, 25.4-mm-thick hot-rolled HY-100 steel provided by the Caderock Division, Naval Surface Warfare Center, was examined in two heat-treatment conditions. In the quenched and tempered condition, the as-received plate had been austenized at 900 °C, quenched, and tempered at 593 °C. In the slow-cooled condition, the as-received plate was subsequently austenized at 905 °C for 75 minutes and slowly cooled to room temperature in a furnace, at an average cooling rate of approximately 0.02 °C/s, from 905 °C to 200 °C. This latter heat-treatment condition produced the microstructural banding described subsequently. The chemical composition of the plate is shown in Table I. It should be noted that alloying elements such as Ni, Cr, Mn, and Mo increase hardenability.

Chemical analyses within the banded microstructure were performed on a local scale using electron probe microanalysis (EPMA) with wavelength-dispersive spectrometry (WDS) to identify the chemical segregation pattern across a trace of approximately 550 μm in length. The trace, which spans several microstructural bands, was marked with two initial hardness indentations prior to WDS analysis. After the WDS analysis, the specimen was repolished and etched to correlate the chemical segregation pattern to the microstructural banding, using the microhardness indentations as locators. Microhardness measurements were made within the alternating layers on the microstructurally banded microstructure. Microstructural observations were performed using light microscopy and scanning electron microscopy on specimens polished and etched with 2 pct nital solution. Transmission electron microscopy was also performed on foils thinned to perforation using 10 pct perchloric acid and 90 pct acetic acid solution in a PHILIPS* EM420T operating at 120 kV.

*PHILIPS is a trademark of Philips Electronic Instruments Corp., Mahwah, NJ.

The uniaxial stress-strain response of the microstructurally banded HY-100 was determined at room temperature from the compression testing of the cylindrical compression specimens, posessing a one-to-one height-to-diameter ratio[11] (ϕ6.35 $\times$ 6.35 mm), at a strain rate of 10^{-3}/s. Compression specimens were machined from the microstructurally banded plate; the stress axes are defined in Figure 1(a) as longitudinal (L), long transverse (T), and short transverse (S). In order to obtain the deformation response at true compressive strains of $\leq$0.75, friction between the specimen and the polished alumina platens was minimized using a Mo_2Si lubricant and by interrupting testing at plastic-strain increments of 0.25. After interruption, the end faces of the specimen, as well as the platens, were relubricated with Mo_2Si lubricant and then reloaded. The slip behavior of the banded microstructure was examined after the compression testing in the T direction. Before the compression testing, a flat-surface segment was ground and polished on the cylindrical face of the compression specimen; this flat face was parallel to the TS plane depicted in Figure 1(b). After deformation, the slip-line characteristics on the flat surface (TS plane) were subsequently examined using a scanning electron microscope (SEM).

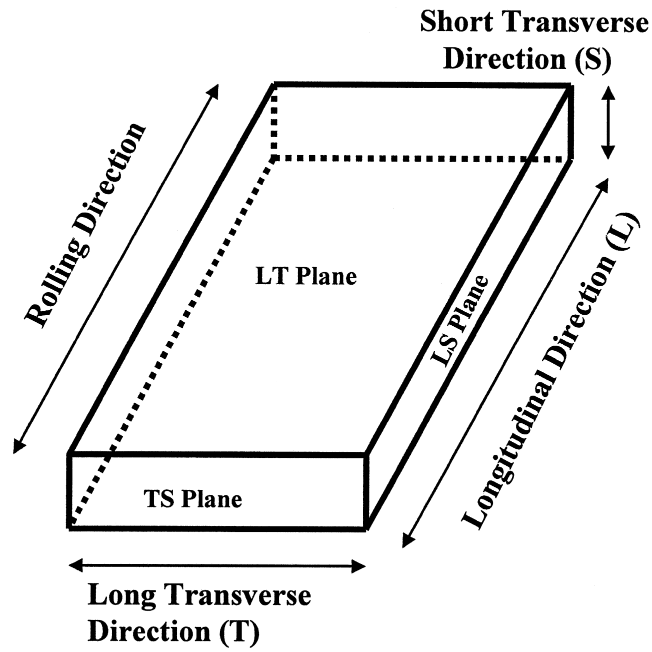

(*a*)

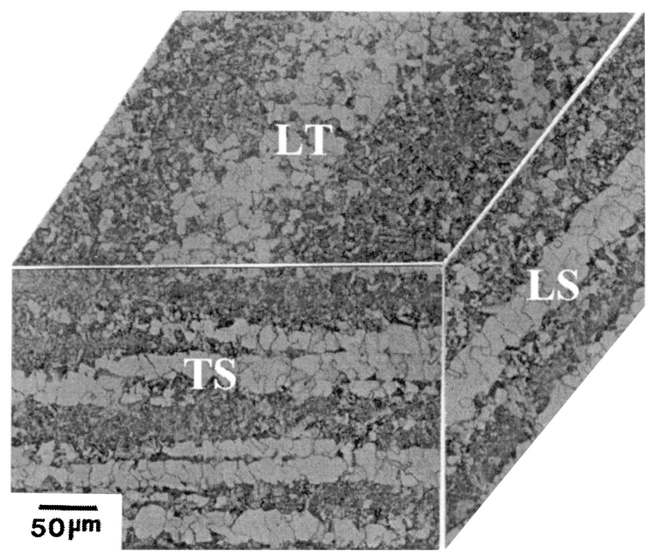

(*b*)

Fig. 1—(*a*) Schematic diagram of the steel plate and (*b*) "three-dimensional light micrograph" showing the microstructural banding in a slow-cooled HY-100 steel.

Tensile testing of circumferentially notched round-bar tensile specimens was conducted to examine the dependence of the failure strain on the degree of stress triaxiality, using a procedure described in detail elsewhere.[9] Testing was conducted at a constant crosshead speed which corresponds to an initial equivalent strain rate of 10^{-3}/s at room temperature. The severity of stress triaxiality was controlled by the geometry of the notch-root radius; the notch geometries used were the so-called B notch (R/ρ = 0.5) and the D notch (R/ρ = 2), where R and ρ are the radius of the minimum

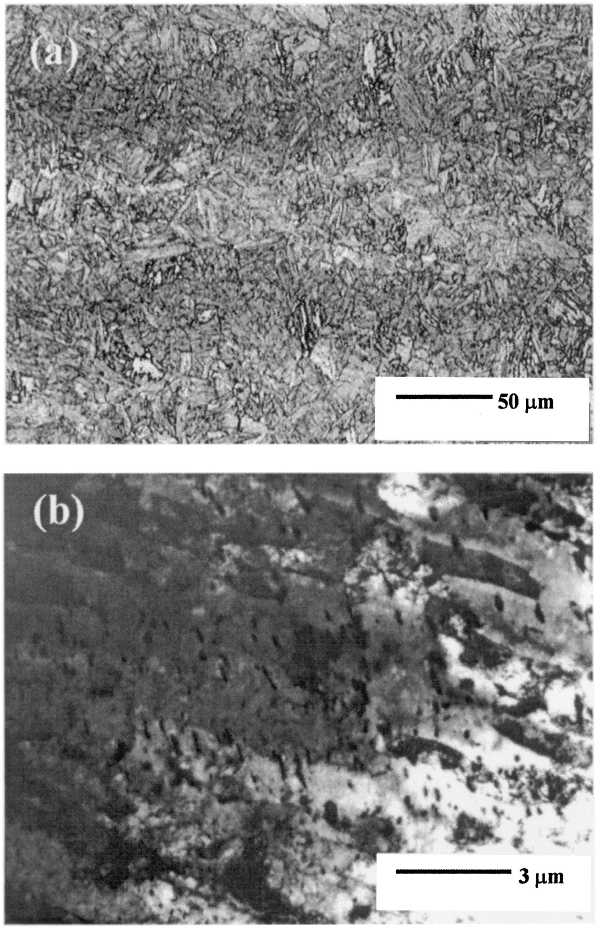

Fig. 2—Microstructures of a hot-rolled HY-100 in the quenched and tempered condition: (*a*) light micrograph showing the faint chemical banding along the rolling direction and (*b*) TEM thin foil micrograph showing tempered martensite microstructure.

cross-sectional area ($2R = 7.62$ mm) and the notch-root radius, respectively. The failure initiation was experimentally defined as a point where the load (P)–diametric contraction (δ) curve showed an abrupt drop during the tensile testing. Having measured the specimen-diameter contraction at failure initiation, we subsequently used finite-element analysis to determine the local stress-strain conditions at the center of the minimum cross-sectional area of the notch where failure initiated. Axisymmetric finite-element analyses were performed for each bar geometry to determine the stress and strain states at failure initiation at the center of the minimum cross-sectional area of the notch. The finite-element-analysis code ABAQUS was used to determine the mean stress (σ_m), equivalent stress (σ_{eq}), and equivalent plastic strain (ε_{eq}), to identify the failure-initiation condition in terms of the stress-triaxiality ratio (σ_m/σ_{eq}) and the equivalent plastic failure strain ($\varepsilon_{f,eq}$) at the failure-initiation site. Fractography was performed after tensile testing using an SEM.

III. RESULTS AND DISCUSSIONS

A. *Microstructure*

The microstructure of the *as-received* quenched and tempered plate of the LS plane is shown in Figure 2(a). The etching contrast is not uniform, with diffuse dark bands running parallel to the rolling direction of the plate. The microstructure consists of tempered martensite (Figure 2(b)) in which fine martensite laths are present, containing a population of closely spaced submicron carbides. The variation in size and shape of both the martensite laths and carbides is demonstrated in Figure 2(b). The boundaries between the laths are not clearly delineated due to the tempering. Despite the difference in the etching contrast in the light micrograph in Figure 2(a), no significant microstructural differences could be detected between several regions when viewed in the SEM or the transmission electron microscope (TEM).

The microstructure of a *furnace-cooled* specimen is characterized by a distinct microstructurally banded array consisting of alternating layers of two quite different microconstituents, as shown in Figure 1(b). The regions of light contrast in Figure 1(b) appear as dark regions in the SEM image and correspond to equiaxed ferritic grains (Figure 3(a)). Carbides are not observed within the ferritic grains at either the SEM or TEM resolution, and only a small population of small (<1 μm) equiaxed MnS inclusions are found within the equiaxed ferrite. The dark-etching layers in Figure 1(b) are imaged as bright regions in the SEM and consist of regions denoted as "granular ferrite" (Figures 3(b) and (c)). The granular ferrite is characterized mainly by the presence of islands of secondary microconstituents within equiaxed ferrite grains (Figure 3(c)).[12] The islands of secondary microconstituents found in the slow-cooled HY-100 consist of martensite or/and austenite, lower bainite, and degenerate pearlite, as indicted by the arrows in Figure 3.

Microstructural banding of steels originates from the interdendritic segregation of substitutional alloying elements in an as-solidified microstructure.[3] In commercial steels, this chemical inhomogeneity persists in the wrought product despite "homogenization," because the diffusion coefficients of substitutional alloying elements in austenite are low. Most studies of microstructural banding have been concentrated on hot-rolled, low-alloy steels,[1–7] and the banding in these steels typically takes the form of alternating layers of ferrite and pearlite. In the present study and in a related study,[14] the banding results in equiaxed ferrite-granular ferrite layers during slow cooling, as is evident in Figure 3.

The cooling rate has been recognized as a main factor in inducing microstructural banding, because the driving force for microstructural banding increases as the cooling rate decreases. For example, Kirkaldy *et al.* showed that the driving force for the microstructural banding is related to the temperature differences between the A_{r3} temperatures (the $\gamma/\gamma + \alpha$ solvus temperature during cooling) of the solute-lean and the solute-rich regions.[1] Their analysis predicts that if the solute lowers the A_{r3} temperature, then proeutectoid ferrite forms first within the solute-lean regions. Based on this reasoning, the layers of equiaxed ferrite present in our banded microstructure should form within a solute-lean region. The subsequent growth of proeutectoid ferrite toward the solute-rich region is accompanied by the diffusion of carbon (an austenite stabilizer) toward the solute-rich (austenite stabilized) region. Finally, the decomposition of the remaining austenite results in the formation of granular ferrite within the solute-rich region.[14] The "island microconstituents" found in the granular ferrite are likely to be retained austenite or/and martensite, as a result of the

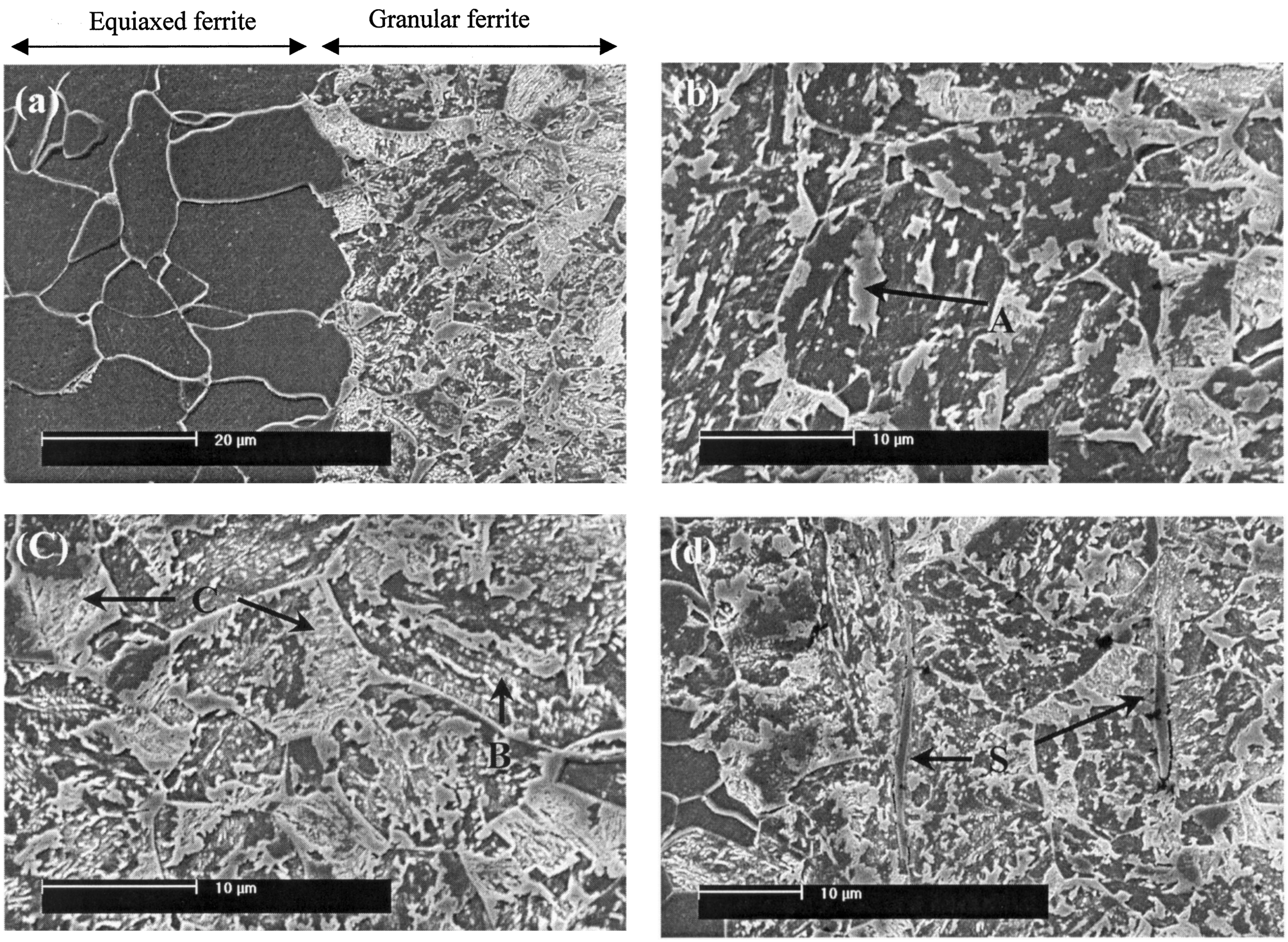

Fig. 3—SEM micrographs showing (*a*) a microstructurally banded microstructure, (*b*) and (*c*) microconstituents in the granular ferrite, and (*d*) elongated MnS inclusions preferentially located within granular ferrite. Arrows indicate "A"—martensite (or retained austenite), "B"—lower bainite, and "C"—degenerate pearlite, while "S" denotes MnS inclusions.

increased carbon and solute (austenite stabilizers) within the granular ferrite regions. However, as will be discussed later, the high hardness of the granular ferrite strongly suggests the presence of martensite as a main secondary microconstituent.

The nature of the chemical segregation rationalized previously is confirmed in Figure 4, which shows the chemical segregation patterns of the substitutional alloying elements, Ni, Cr, Mn, and Mo along a trace $\approx$550 μm long, which spans many microstructural bands (LS plane). The concentration profiles confirm that the equiaxed ferrite forms at the solute-lean region and that Ni, Cr, and Mo concentrate within the layers of granular ferrite. As a result, the segregation patterns are all "in phase."

The microstructural banding present in the slow-cooled HY-100 may be further understood by utilizing the empirical formula for the effect of alloying elements on the critical temperature (A_3):[13]

$$A_3 = 910 - 203\sqrt{C} - 15.2Ni + 44.7Si + 104V + 31.5Mo + 13.1W - 30Mn - 11Cr - 20Cu + 700P + 400Al + 120As + 400Ti$$

It should be noted that Cr lowers the A_3 temperature, as do Ni and Mn. K.W. Andrews pointed out that Cr in the compositional range of 0 to 5 wt pct acts as an austenite stabilizer.[13] Therefore, Ni, Cr, and Mn (austenite stabilizers) lower the A_3 temperature, while Mo (ferrite stabilizer) raises the A_3 temperature. The combined capability of Ni, Cr, and Mn in lowering the A_3 temperature far exceeds the capability of Mo in raising the A_3 temperature. If the ability of each element in lowering the A_3 temperature is considered among the austenite stabilizing elements, then the high content of Ni (2.62 wt pct) is likely to play a key role in producing the microstructural banding in HY-100. Finally, we note that solute-segregation patterns similar to those shown in Figure 4 are also found in the slowly cooled HSLA-100 steel, which is more highly alloyed than HY-100. In HSLA-100, all the substitutional elements (Ni, Cu, Mn, Cr, Mo, and Nb) tend to be concentrated within the layers of granular ferrite.[14]

The degree of the microstructural banding may be quantified on the LT, TS, and LS planes (Figure 1), using the equations as follows:[15]

$$\text{Anisotropy Index} = \frac{\overline{P}_{L\perp}}{\overline{P}_{L\parallel}}$$

$$\text{Degree of Orientation} = \frac{\overline{P}_{L\perp} - \overline{P}_{L\parallel}}{\overline{P}_{L\perp} + 0.571\overline{P}_{L\parallel}}$$

where $\overline{P}_{L\perp}$ is the average number of feature-boundary intersections (in this case, equiaxed ferrite/granular ferrite) with

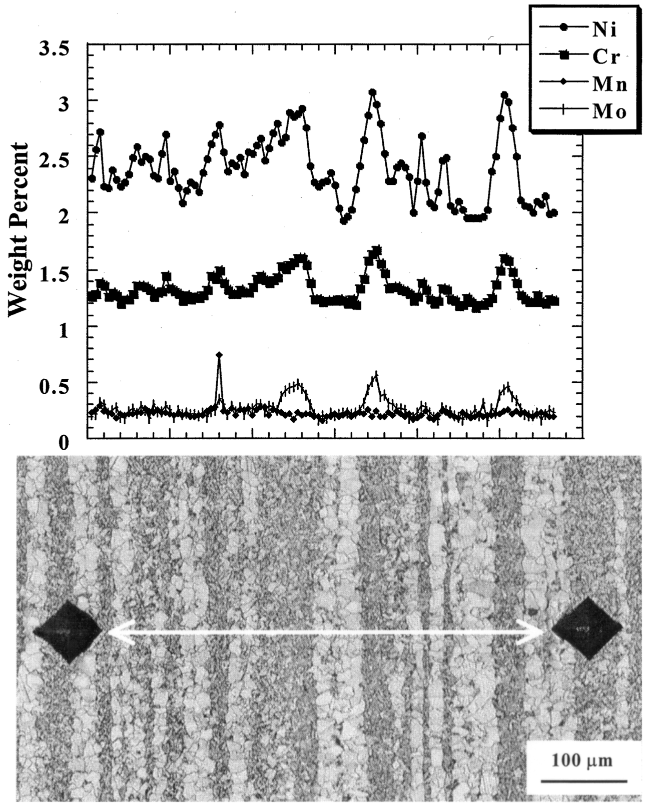

Fig. 4—Correlation between the microstructural banding and the segregation patterns of the alloying elements: the LS surface is shown, and the arrow on the light micrograph indicates the range of the chemical analyses.

Table II. A Quantitative Assessment of the Degree of the Microstructural Banding

Plane	$\overline{P}_{L\perp}$ (number/mm)	$\overline{P}_{L\mu}$ (number/mm)	Anisotropy Index	Degree of Orientation
LT	4.54	1.23	3.69	0.63
TS	40.24	3.85	10.45	0.86
LS	38.48	1.32	29.15	0.95

test lines perpendicular to the banding direction per unit test line length, and $\overline{P}_{L\parallel}$ is the average number of feature-boundary intersections with test lines parallel to the banding direction. For a randomly oriented microstructure, the anisotropy index and the degree of orientation are 1 and zero, respectively. As the anisotropy of the microstructure increases, the anisotropy index increases above 1, and the degree of orientation approaches 1. Table II shows that both the anisotropy index and the degree of orientation are highest on the LS plane and lowest on the LT plane. In addition, the degree of banding is most pronounced (degree of orientation = 0.95) on the LS plane.

The volume fraction (V_f) of the granular ferrite was also measured on the LS and TS planes and was determined to be $V_f = 0.42$. The mean edge-to-edge spacing of the granular ferrite layers (mean free path) was used to estimate the average thickness of the carbide-free ligaments on the LS and TS planes, using the obtained volume fraction of granular ferrite ($V_f = 0.42$). Assuming the same volume fraction on the LT plane, the average thickness of the carbide-free

Table III. A Quantitative Analysis of the Microstructurally Banded HY-100

Plane	Volume Fraction of Granular Ferrite	Center to Center Band Spacing (μm)	Average Thickness of Carbide-Free Ligament (μm)	Average Thickness of Granular Ferrite (μm)
LT	—	441	256	185
TS	0.42	50	29	21
LS	0.42	52	30	22

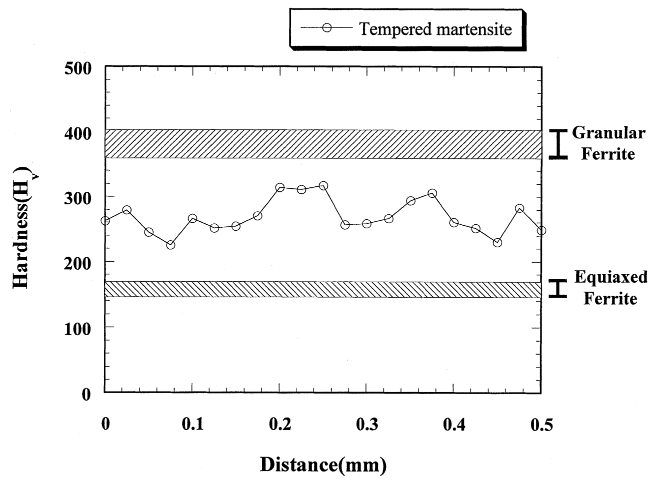

Fig. 5—Hardness profiles of a quenched and tempered HY-100 on the LS plane. Hardness bands for equiaxed ferrite and granular ferrite are also shown.

ligaments (proeutectoid ferrite widths) was also estimated (Table III).

In summary, based on the previous quantitative analyses, the simplified three-dimensional picture of the banded microstructure is as follows: the layers of the granular ferrite themselves assume an elongated "pancake" shape, having their major dimension aligned along the rolling direction and the minor axis in the through-thickness direction. The bands consist of alternating layers of granular ferrite, roughly 20 μm in thickness, and carbide-free equiaxed ferrite, approximately 30 μm in thickness.

B. *Hardness Behavior*

Given the large difference in the microstructures between the banded regions in the slow-cooled HY-100 steel, it is not surprising that their hardness values would also be significantly different. In fact, the Vickers hardness (VHN) of the granular ferrite layers (VHN = 374) is more than twice that of the equiaxed ferrite (VHN = 159). The high hardness value of the granular ferrite suggests the presence of hard martensite islands, which have often been found in granular microstructures.[12] Thus, the microstructural banding has resulted in alternating layers with quite different hardnesses and, presumably, flow behaviors. Ramifications of such a microstructure will be discussed later.

While there are large microhardness variations within HY-100 in the slow-cooled condition, the quenched and tempered condition also exhibits a nonuniform hardness profile, as depicted in Figure 5. The average hardness value for the quenched and tempered condition is 269 VHN; however, hardness differences of approximately 90 VHN are present. Furthermore, the wavelength of the hardness variations corresponds approximately to the chemical banding of the substitutional elements seen in Figure 4. Thus, although the chemical banding does not result in distinctly different microstructures in the quenched and tempered condition, it nevertheless remains present and results in local variations of hardness values.

Finally, based on the respective hardnesses of the equiaxed and granulate ferrites and the volume fraction of each ($V_{f,\text{granular ferrite}} = 0.42$), we may estimate the *macroscopic* hardness of the banded, slow-cooled steel using a straightforward law-of-mixtures relationship based on the respective volume fractions of equiaxed and granular ferrite. Recalling that the equiaxed and granular ferrite hardnesses were 159 and 374 VHN, respectively, a law-of-mixtures relationship predicts the average hardness of the microstructurally banded material to be 250 VHN, or somewhat less than that of the tempered martensitic material (269 VHN). Using Rockwell B measurements (HRB) as macrohardness data, we find a similar correspondence of hardnesses for these two microstructures; *i.e.*, HRB = 95.4 ($\approx$216 VHN) for the banded structure compared to HRB = 99.9 ($\approx$240 VHN) for the tempered martensite.

C. *Compression Response and Slip-Line Behavior*

Figure 6 shows the compressive stress-strain responses determined on the microstructurally banded HY-100 in the three orthogonal loading directions. The microstructural change from the tempered martensite to the equiaxed ferrite–granular ferrite banded structure results in a decrease in the yield stress of about 20 pct, from $\approx$650 MPa to the 500 to 530 MPa range. With increasing strain, the flow-stress differences between these two microstructures decrease. As is evident in Figure 6, the banded structure displays higher strain hardening, such that the flow stresses approach that of the tempered martensite at large strains. If the stress-strain response is fitted to a power-law relationship, the strain-hardening exponent ($n = d \ln \sigma / d \ln \varepsilon$) increases from 0.09 in the quenched and tempered condition to 0.12 to 0.14 in the slow-cooled condition (Table IV). Finally, we note that small differences in strain hardening among the three orientations of the slow-cooled, banded structure result in significant differences in their flow stresses at large strains; we will return to this issue later.

The deformation of coarse two-phase microstructures depends on whether the material obeys an equal-stress condition (in which strain can concentrate in one of the microconstituents) or if an *equal strain* condition applies to the constituents. Given the layered morphology of the microstructure (Figure 1), we would expect the equal-strain condition to be obeyed for deformation with the compression axes along the L and T directions, but that perhaps this requirement might be relaxed in the S direction. Interestingly, the stress-strain responses in the three loading directions of the microstructurally banded material (Figure 6) are very similar up to strains of $\approx$0.1, suggesting that the compatibility constraints are such that both the equiaxed and granular ferrites are forced to deform in an equal strain manner.

The higher degree of work-hardening observed for the slow-cooled material suggests an increased rate of dislocation accumulation with strain. One possibility is an elevated rate of dislocation accumulation within the softer equiaxed ferrite, due to strain compatibility requirements arising from the presence of the harder, but still ductile, granular ferrite. Such a suggestion is similar to reasoning used in describing the very high strengths developed in the heavily deformed

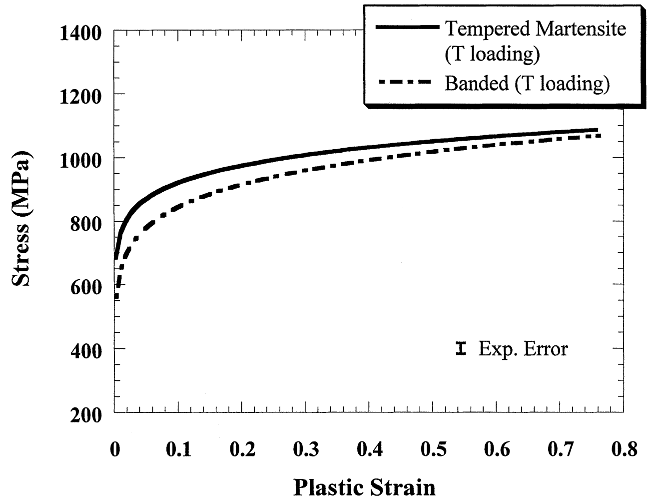

(*a*)

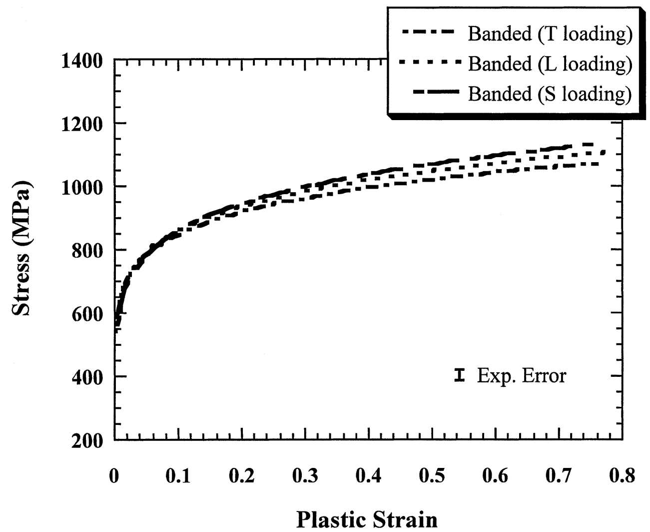

(*b*)

Fig. 6—Compressive stress-strain responses for (*a*) the T loading of the microstructurally banded and the quenched and tempered materials and (*b*) the microstructurally banded material in the three orthogonal loading directions.

Table IV. A Summary of the Compressive Stress-Strain Responses (We Assume $\mu = K\varepsilon^n$)

Microstructure	Tempered Martensite	Equiaxed Ferrite and Granular Ferrite Banding		
Loading direction	T	T	L	S
n	0.09	0.12	0.13	0.14
K (MPa)	1134	1104	1140	1173
0.2 pct yield stress (MPa)	648	536	526	501

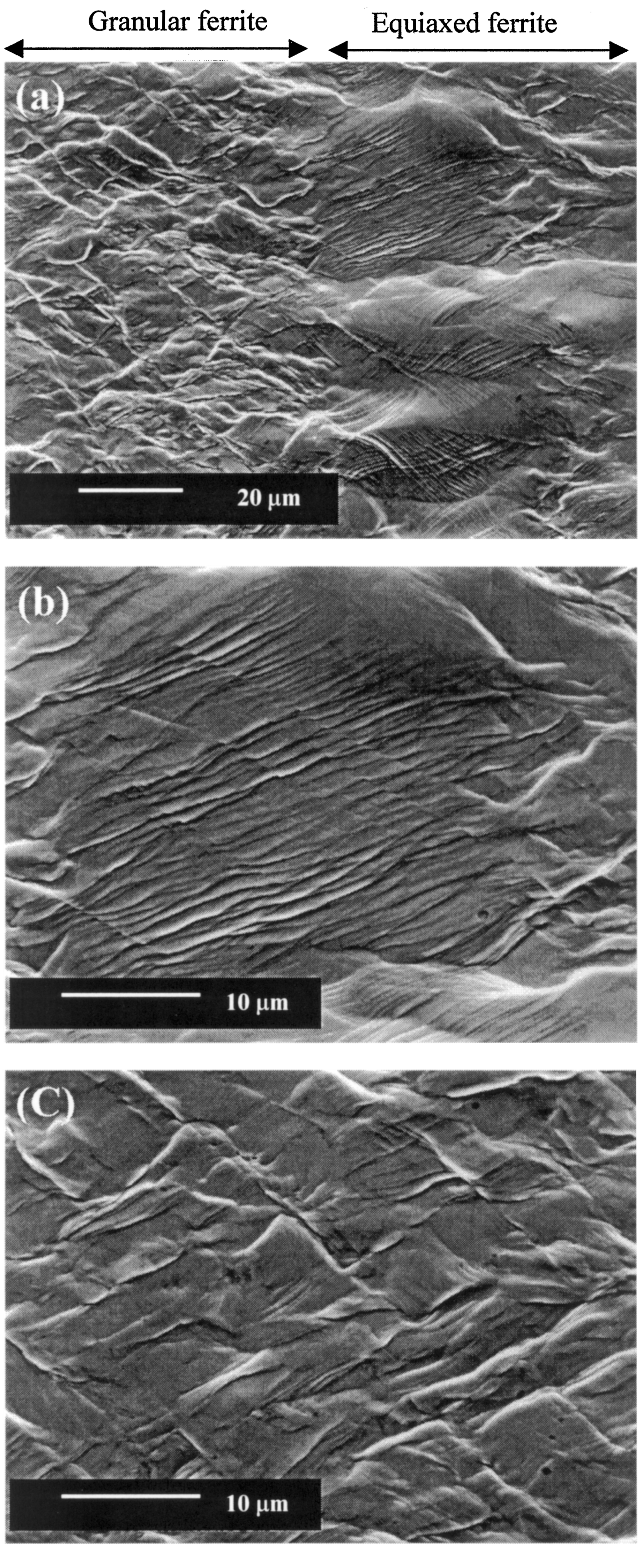

Fig. 7—Slip line behavior in the microstructurally banded steel: (*a*) both microconstituents, (*b*) the equiaxed ferrite only, and (*c*) the granular ferrite only. The macroscopic strain is 0.5. The stress axis is vertical and corresponds to the T direction (Fig. 1).

two-phase Cu-based alloys, examined by Courtney and coworkers a decade ago.[16,17] Figure 7 provides indirect support for such speculation in the characteristics of the slip traces at a 0.5 strain. In particular, an examination of the slip behavior, such as that depicted in Figure 7(a), suggests that slip accommodation is occurring within the softer equiaxed ferrite to accommodate the deformation behavior of the harder granular ferrite. Furthermore, while the slip bands tend to be oriented at roughly 45 deg to the stress axis, the slip lines are finely spaced and wavy in the equiaxed ferrite (Figure 7(b)), but are widely spaced, coarse, and planar in the hard granular ferrite (Figure 7(c)). We may speculate that such slip compatibility behavior results in an increased dislocation density within the equiaxed ferrite, which contributes to the increased strain hardening of the slow-cooled banded microstructure steel.

The strain-hardening behavior of the banded microstructure in Figure 6(b) indicates small but significantly different flow stresses at large strains among the three specimen orientations. This result implies a strain-induced anisotropy of deformation, a result of which is that the cross sections of the compression specimens do not remain circular at large strains. This effect is demonstrated in Figure 8, which shows the cross-sectional geometry and the corresponding microstructures of three compression specimens, each having a different loading direction. While the cross section of the specimen deformed in the S direction remains circular (Figure 8(a)), the cross sections of the specimens oriented in the two other plate directions become distinctly elliptical (Figures 8(b) and (c)). As expected, these observations indicate that material flow is constrained by the harder granular ferrite bands in the banding direction (*i.e.*, the long dimension of the band layer).

In order to quantify the anisotropy of the flow behavior in Figures 8(b) and 8(c), we define a strain ratio (R) such that $R = \varepsilon_2/\varepsilon_3$, where ε_2 and ε_3 are the minor and major principal strains transverse to the compression axis, respectively. (Such a strain ratio relates directly to that often used to describe the plastic anisotropy of sheet metal, in which $R = \varepsilon_{\text{width}}/\varepsilon_{\text{thickness}}$ in a uniaxial tension test.) As also shown in Figure 8, the strain ratios measured from the compression specimens tested in the S, L, and T loading directions are 0.98, 0.89, and 0.77, respectively, at a true compressive strain of 0.75. These ratios may be qualitatively understood in terms of the geometry of the banding present in the slow-cooled microstructure. The smallest R value (0.77), or the greatest degree of plastic anisotropy, is observed when the material is deformed in the T direction of the plate, which can be readily reconciled in terms of constraint imposed by the layers of hard granular ferrite, given the structures shown in Figure 1. In contrast, when the loading direction is in the S direction, the strain ratio is $R \approx 1$, which implies that the plastic deformation of the banded material is orthotropically isotropic, transverse to the compressive axis.

D. *Tensile Behavior under Multiaxial Tension*

In a previous study, we have examined the failure of a quenched and tempered HY-100 steel plate as a function of stress state using notched axisymmetric tensile specimens.[9,10] These results show that, if the specimen is tested in the T direction, increasing stress triaxiality results in a rapid decrease in failure strains. Furthermore, at high-stress triaxialities, failure is controlled by a void-sheet process which links large elongated, inclusion-initiated voids by a shear instability process. In contrast, when tested in the L direction, failure of the HY-100 steel plate is controlled by

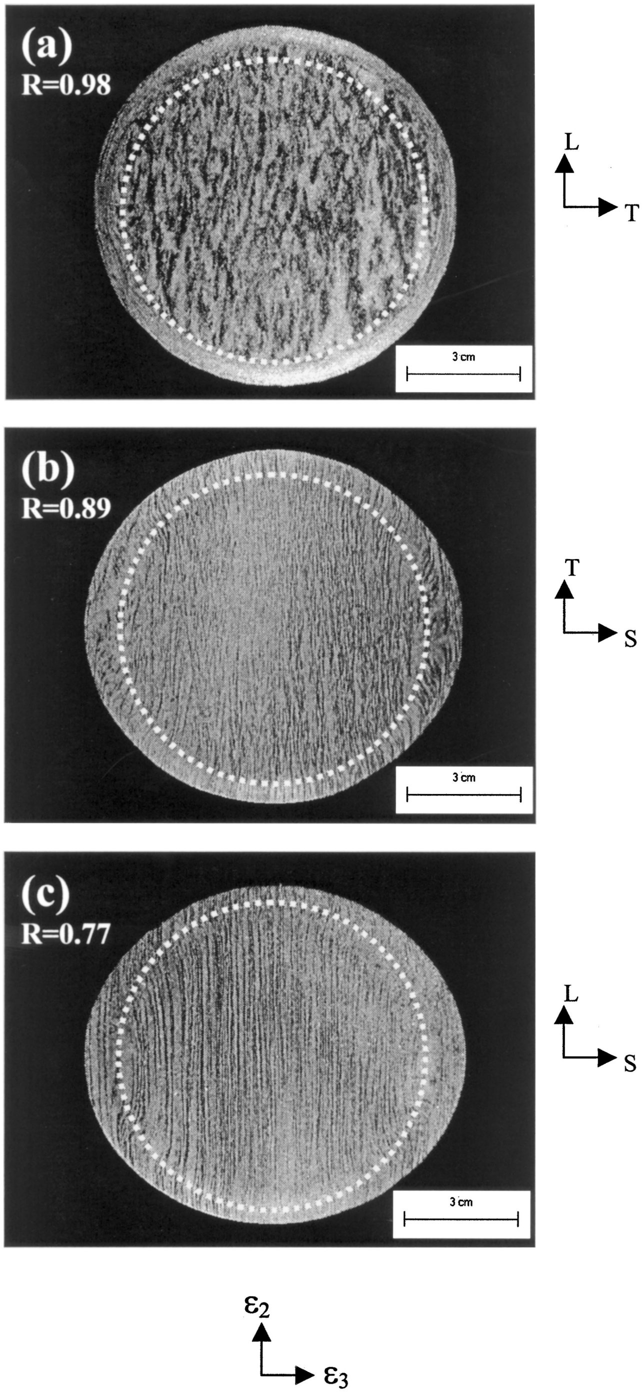

Fig. 8—Light micrographs of the polished and etched surfaces of the end faces of the compression specimens. The white dotted circles serve to illustrate the flow anisotropy in the three loading directions: (*a*) S, (*b*) L, and (*c*) T.

the growth and coalescence of equiaxed voids. In this section, we compare the behavior of the banded slow-cooled material to that examined earlier (the quenched and tempered material).

As before,[9,10] we define material "failure" as that condition in which material damage is sufficiently severe such that a measurable loss of stress-carrying capacity of the material occurs as deformation continues. Experimentally, we determined failure initiation from load-displacement data

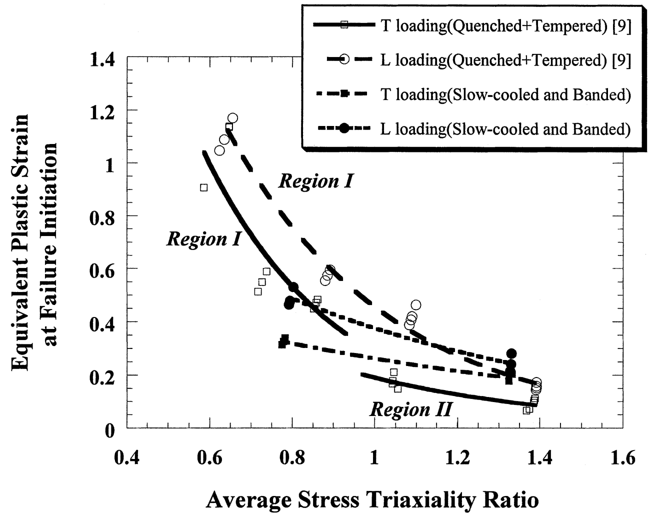

Fig. 9—Comparison of the failure limit data for the tempered martensite and the microstructurally banded HY-100 steels.

as the point where the load-diametric contraction curve changes abruptly during the deformation. We used finite-element analysis in order to determine the condition at failure, as represented by the stress-triaxiality ratio and equivalent plastic strain at the center of a notched bar; note that σ_m is the mean stress and σ_{eq} is the equivalent stress. During a notched-bar test, there is a (small) change in the stress-triaxiality level as the specimen deforms, due to a changing notch geometry. We, thus, define an average stress triaxiality over the strain interval to failure initiation as follows:[9,10]

$$(\sigma_m/\sigma_{eq})_{\text{average, failure}} = \frac{\int (\sigma_m/\sigma_{eq})\, d\varepsilon_{eq}}{\int d\varepsilon_{eq}}$$

In order to address the possible effect of microstructural banding on initiating void-sheet failure, we have chosen two round-notched tensile-specimen geometries: a high-stress-triaxiality *D*-notch ($\sigma_m/\sigma_{eq} \approx 1.4$) and a low-stress-triaxiality *B*-notch configuration ($\sigma_m/\sigma_{eq} \approx 0.8$). These specimens were tested in both the T and the L directions of the plate. It should be recognized that the void-sheet mechanism is prevalent only when the quenched and tempered HY-100 is tested in the T direction *and* at high-stress-triaxiality ratios ($1.0 < \sigma_m/\sigma_{eq} < 1.4$).[8,9,10]

1. *Loading in the T orientation of the plate*

The dependence of the failure strains on the stress state, as depicted in the failure-limit diagram (FLD) in Figure 9, is shown for both the microstructurally banded and the quenched and tempered HY-100 steels. In the latter case, for specimens tested in the T direction, the FLD data in Figure 9 are separated into two regions. Previous research[8,9,10] has shown that these two regions relate to two failure mechanisms: a damage accumulation process involving coalescence of relatively equiaxed voids (region I in Figure 9) and a void-sheet process, which links the large, elongated inclusion-initiated voids by localization of deformation (region II in Figure 9).

Comparing the response of the slow-cooled, banded steel to the tempered martensitic case, we observe several significant trends. First, the microstructurally banded material

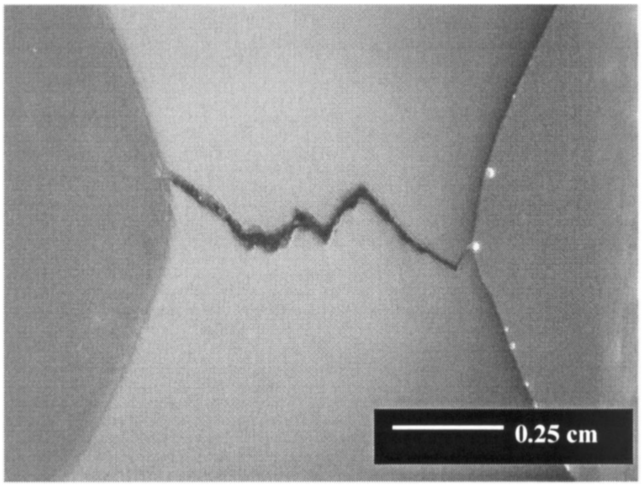

Fig. 10—Profile of the fracture path in a microstructurally banded steel tested in the long transverse direction of the plate. Stress triaxiality is approximately 0.75.

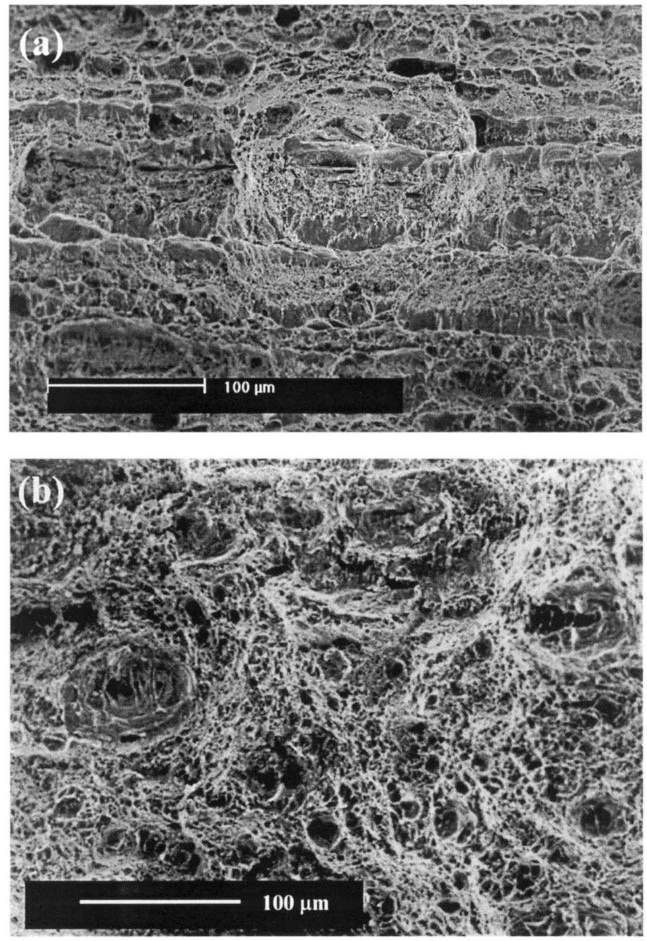

Fig. 11—Fracture surface appearances after failure at intermediate stress triaxiality ($\sigma_m/\sigma_{eq} \approx 0.75$): (*a*) microstructurally banded and (*b*) tempered martensite.

shows a "region II" sensitivity of failure strains to stress state, for the entire range of stress triaxialities ($0.8 < \sigma_m/\sigma_{eq} < 1.4$) examined. This behavior is in contrast to the failure of the quenched and tempered specimens, where region II failure is confined to high-stress triaxialities ($1.0 < \sigma_m/\sigma_{eq} < 1.4$). Second, the failure strains of the banded material are larger at the high-stress triaxialities ($1.0 \leq \sigma_m/\sigma_{eq} \leq 1.4$), but, as a result of the persistence of region II behavior, they are lower than the tempered material at the $\sigma_m/\sigma_{eq} \cong 0.8$ level. Thus, there is a "crossover" of failure strains, such that the quenched and tempered martensitic material has greater resistance to failure at intermediate-stress-triaxiality levels.

An obvious interpretation to the aforementioned FLD data (Figure 9) is that the banded microstructure extends the void-sheet mode of failure to the lower-stress triaxialities. Recalling that void sheeting occurs due to a shear localization at the ligament between elongated MnS inclusions, the fracture path shown in Figure 10 for the banded steel is not surprising; this figure clearly indicates a susceptibility of failure to planes inclined at ≈45 deg to the tensile axis. In view of Figure 9 and our previous interpretation of regions I and II,[8,9,10] we now anticipate that the fractography of the quenched and tempered and slow-cooled steels should show distinctly different fracture surfaces at the intermediate-stress-triaxiality conditions. Figure 11 confirms this expectation. In Figure 11(a), we see that the failure surface of the banded steel is dominated by an aligned "ridge-trough" fracture surface in which elongated primary voids are linked by planes of microvoids; all of these features are characteristic of void-sheet failure. In contrast, the quenched and tempered steel in Figure 11(b) shows equiaxed dimples which have formed as a result of equiaxed voids, which have grown and coalesced by impingement in what we have previously termed region I failure. In summary, both the fracture-surface profiles and fractography confirm that the banded material is *more* susceptible to void-sheet failure than the tempered martensitic steel at the intermediate stress-triaxiality levels in Figure 9.

A straightforward interpretation of the void-sheet mode of failure in HY-100 steel is that the MnS inclusions, which are preferentially located within the granular ferrite layers, initiate large elongated voids that, in turn, trigger deformation localization between them, *on a 45-deg inclined plane*, between the layers of granular ferrite. The final stage of the void-sheet failure process of the quenched and tempered martensitic HY-100 is believed to involve the nucleation and coalescence of voids at the submicron carbides present within the bands of deformation localization between the primary voids. As shown in Figure 12(a), the fracture surface of the slow-cooled, banded steel consists of three types of voids: (1) the large primary voids associated with the elongated MnS inclusions within the granular ferrite, (2) a large number of small, equiaxed voids nucleated from the equiaxed MnS inclusions (approximately 1 to 2 μm in diameter) concentrated near the large, elongated MnS inclusions, and (3) large, equiaxed voids nucleated within the equiaxed ferrite and at the boundary between the equiaxed and granular ferrites (Figure 12(b)). The first two types of voids are also observed in the quenched and tempered material, which is understandable, given that the heat treatment performed in this study should not produce any significant change in the inclusion shape, size, or location.

The third type of void described previously (*i.e.*, the large equiaxed voids in the soft ferrite) is unique to the microstructurally banded steel. Since the layer of the equiaxed ferrite contains few carbides, void nucleation is inhibited and must

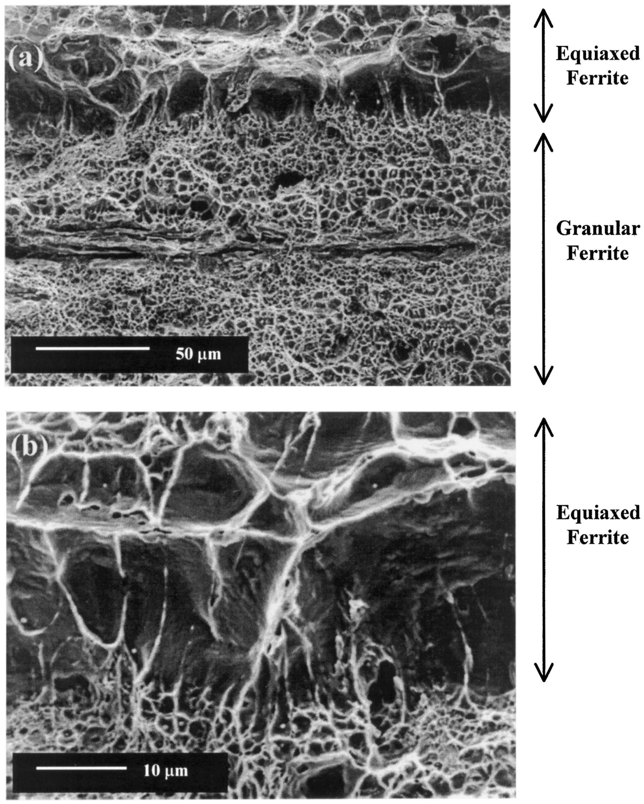

Fig. 12—(*a*) and (*b*) Fractographs showing void-sheet failure in the slow-cooled banded steel when the tensile axis is in the T direction of the plate. Stress triaxiality is approximately 1.3.

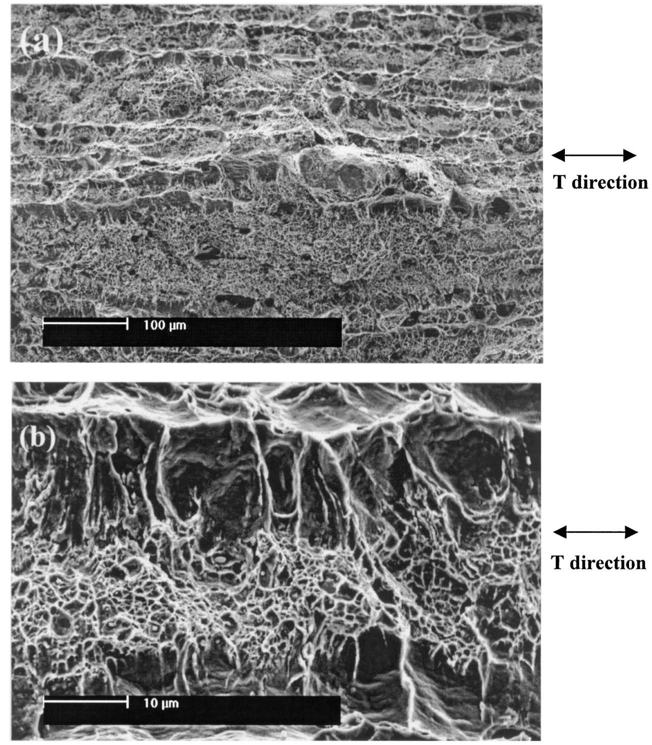

Fig. 13—(*a*) and (*b*) Fractographs showing void-sheet failure in a slow-cooled steel specimen when the tensile axis is in the L direction of the plate. Stress triaxiality is approximately 1.3.

rely on slip intersection and/or the small population of small, equiaxed MnS inclusions. Although void nucleation from small, equiaxed MnS inclusions within the layer of the equiaxed ferrite was detected (Figure 12(b)), the population of such inclusions is small, and the result is that relatively few voids nucleate within the equiaxed ferrite, but these voids grow to a large size prior to impingement.

Taken as a whole, the fractographic observations described previously for tensile loading in the T orientation of the plate are consistent with the implied extension of the void-sheeting suggested by the FLD data in Figure 9. The aligned nature of the hard granular ferrite regions within which the elongated MnS inclusions are embedded (and oriented normal to the stress axis) favors nucleation of elongated primary voids and the retention of a local plane-strain condition in their vicinity. The result is an extension of the void-sheet mode of failure to intermediate-stress triaxialities. The absence of carbides within the equiaxed ferrite between the primary voids delays the failure of the ligaments between the primary voids to larger failure strains, as is also observed in Figure 9.

2. *Loading parallel to the rolling direction, i.e., L loading*

When the slow-cooled, microstructurally banded steel is tested in the L direction of the plate, the dependence of the failure strains on stress triaxiality is similar to that in the T direction, and, in turn, similar to region II behavior of the quenched and tempered specimens tested in the T direction.[8,9,10] As shown in Figure 9, these data imply that even in the *longitudinal* loading orientation, the void sheet-type failure mechanism may prevail at intermediate-to-high–stress triaxialities in the slow-cooled material. Such a result is somewhat unexpected, because the void-sheet mode of failure has been considered likely *only* when the loading is in the T direction of the hot-rolled plate, in which case the elongated voids (nucleated from the elongated MnS inclusion) are oriented perpendicular to the loading axis.[8,9,10]

The presence of a void-sheet mode of failure, even in the L specimens, is supported by observations such as Figure 13, which shows that, even though the elongated MnS nucleated voids are not present, the ridge-trough fracture path, a characteristic of the void-sheet mode of failure, is still observed. Furthermore, specimen-tilting experiments in the SEM confirmed that planar sections of the fracture surface were, indeed, inclined at angles roughly 45 deg to the tensile axis.

The observations described previously imply that, despite the *absence* of elongated MnS-initiated voids oriented normal to the tensile axis, the void-sheet mode of failure still controls the failure of the longitudinally loaded HY-100 in the slow-cooled, banded condition. This somewhat surprising result may be understood, at least qualitatively, as follows. One of the criteria suggested previously for void-sheet failure is a *local* plane-strain condition for deformation created along the long direction of the MnS inclusions.[8] Such a stress state is normally established on a microscale between elongated, "cigar-shaped" voids created by failure of MnS inclusions oriented normal to the tensile axis.[8] For the case of a longitudinally oriented steel, the voids initiated at MnS inclusions have an equiaxed shape, as shown within the granular ferrite in Figure 13(b). Nevertheless, it seems plausible that void-sheet failure may still occur in the following manner. At small strain levels, the high density of MnS particles concentrated in the hard granular ferrite nucleate equiaxed voids. The voided granular ferrite deforms by localized planar slip (such as in Figure 7(c)), but in such a manner that the aligned nature of the granular ferrite bands (Figure 1) restricts deformation along their length (as shown in Figure 8(b)) *and promotes a local plane-strain condition*. Thus, the voided granular ferrite appears to create the conditions for shear localization and eventual failure on zigzagged planes of high shear stress connecting the bands. A form of void-sheet failure results, although the absence of the elongated voids delays the onset of deformation localization. Failure in the L orientation, thus, exhibits more ductility than that in the T loading orientation (Figure 9).

IV. SUMMARY

Local chemistry variations which persist in hot-rolled HY-100 steel plate induce pronounced microstructural banding upon slow cooling from the austenite region. The resulting microduplex banded structure consists of alternating layers of soft equiaxed ferrite and hard granular ferrite, the latter assuming an elongated, pancake-shaped morphology with the major dimension aligned in the rolling direction and the minor axis oriented in the through-thickness direction of the plate. Given a microstructure containing martensite and/or austenite, bainite, and degenerate pearlite, the granular ferrite is much harder than the equiaxed ferrite, which forms carbide-free ligaments. One consequence of the microstructural morphology is anisotropic deformation during uniaxial compression, as the layers of hard granular ferrite constrain plastic flow along their length.

Circumferentially notched tensile specimens have been used to explore the failure behavior as a function of stress triaxiality. For specimens oriented in both the T *and* the L directions of the plate, the slow-cooled, microstructurally banded steel shows a pronounced susceptibility to the void-sheet mode of failure. The failure strains are limited and exhibit a weak sensitivity on stress triaxiality as MnS-initiated voids (located in the granular ferrite) link due to shear localization (primarily within the equiaxed ferrite) along planes inclined at roughly 45 deg to the tensile axis. However, the absence of finely spaced carbides within the equiaxed ferrite inhibits void nucleation and delays void coalescence, and specimen failure of the slow-cooled steel usually occurs at higher strains than in the quenched and tempered counterpart. The presence of the void-sheet mode of failure, when the slow-cooled steel is loaded in the L direction of the plate, is somewhat surprising, since it occurs despite the *absence* of elongated MnS-initiated voids oriented normal to the tensile axis. Such an observation suggests that the aligned morphology of the harder granular ferrite, and the resulting plastic constraint along its length, promote the local plane-strain condition believed to be necessary for void linking by the void-sheet mechanism.

ACKNOWLEDGMENTS

We are grateful to Jeremy Crawford for his experimental help and to Dana Goto and J.P. Bandstra for their valuable discussions. The Office of Naval Research and the Naval Surface Warfare Center funded most of this research. One of the authors (ALW) acknowledges the support of the Applied Research Laboratory, Penn State University.

REFERENCES

1. J.S. Kirkaldy, J. von Destinon-Forstmann, and R.J. Brigham: *Can. Metall. Q.*, 1962, vol. 1, pp. 59-81.
2. J.S. Kirkaldy, R.J. Brigham, H.A. Domian, and R.G. Ward: *Can Metall. Q.*, 1963, vol. 2, pp. 233-41.
3. E.T. Turkdogan and R.A. Grange: *J. Iron Steel Inst.*, 1970, vol. 208, pp. 482-94.
4. S.W. Thompson and P.R. Howell: *J. Mater. Sci. Technol.*, 1992, vol. 8, pp. 777-84.
5. J.A. Eckert, P.R. Howell, and S.W. Thompson: *J. Mater. Sci.*, 1993, vol. 28, pp. 4412-20.
6. R.A. Grange: *Metall. Trans.*, 1971, vol. 2, pp. 417-26.
7. W.A. Spitzig and R.J. Sober: *Metall. Trans. A*, 1981, vol. 12A, pp. 281-91.
8. J.P. Bandstra, D.M. Goto, and D.A. Koss: *Mater. Sci. Eng. A*, 1998, vol. A249, pp. 46-54.
9. D.M. Goto, D.A. Koss, and V. Jablokov: *Metall. Mater. Trans. A*, 1999, vol. 30A, pp. 2835-42.
10. D.M. Goto, D. Chae, and D.A. Koss: *Progress in Mechanical Behavior of Materials*, Fleming Printing, Victoria, BC, Canada, 1999, vol. 1, pp. 150-54.
11. M.L. Lovato and M.G. Stout: *Metall. Trans. A*, 1992, vol. 23A, pp. 935-51.
12. S.W. Thompson, D.J. Colvin, and G. Krauss: *Metall. Trans. A*, 1990, vol. 21A, pp. 1493-1507.
13. K.W. Andrews: *J. Iron Steel Inst.*, 1965, vol. 203, pp. 721-27.
14. D. Chae, D.A. Koss, A.L. Wilson, and P.R. Howell: The Pennsylvania State University, University Park, PA, unpublished research, 1999.
15. *Annual Book of ASTM Standards*, ASTM Designation E 1268-94, 1996, vol. 3.01.
16. P.D. Funkenbusch and T.H. Courtney: *Acta Metall.*, 1985, vol. 33, pp. 913-22.
17. P.D. Funkenbusch, J.K. Lee, and T.H. Courtney: *Metall. Trans. A*, 1987, vol. 18A, pp. 1249-56.